
Article:
Chekhovich, E.A., Ulhaq, A., Zallo, E. et al. (3 more authors) (2017) Measurement of the spin temperature of optically cooled nuclei and GaAs hyperfine constants in GaAs/AlGaAs quantum dots. Nature Materials, 16 (10). pp. 982-986. ISSN 1476-1122

https://doi.org/10.1038/nmat4959

Measurement of the spin temperature of optically cooled nuclei and GaAs hyperfine constants in GaAs/AlGaAs quantum dots

E. A. Chekhovich[1], A. Ulhaq[1], E. Zallo[2,3], F. Ding[2], O. G. Schmidt[2], and M. S. Skolnick[1]
[1] *Department of Physics and Astronomy, University of Sheffield, Sheffield, S3 7RH, United Kingdom.*
[2] *Institute for Integrative Nanoscience, IFW Dresden, Helmholtz str. D-01069, Dresden, Germany. and*
[3] *Paul-Drude-Institut für Festkörperelektronik, Hausvogteiplatz 5-7, 10117 Berlin, Germany.*

Deep cooling of electron and nuclear spins is equivalent to achieving polarization degrees close to 100% and is a key requirement in solid state quantum information technologies [1–7]. While polarization of individual nuclear spins in diamond [2] and SiC [3] reaches 99% and beyond, it has been limited to 50-65% for the nuclei in quantum dots [8–10]. Theoretical models have attributed this limit to formation of coherent "dark" nuclear spin states [11–13] but experimental verification is lacking, especially due to the poor accuracy of polarization degree measurements. Here we measure the nuclear polarization in GaAs/AlGaAs quantum dots with high accuracy using a new approach enabled by manipulation of the nuclear spin states with radiofrequency pulses. Polarizations up to 80% are observed – the highest reported so far for optical cooling in quantum dots. This value is still not limited by nuclear coherence effects. Instead we find that optically cooled nuclei are well described within a classical spin temperature framework [14]. Our findings unlock a route for further progress towards quantum dot electron spin qubits where deep cooling of the mesoscopic nuclear spin ensemble is used to achieve long qubit coherence [4, 5]. Moreover, GaAs hyperfine material constants are measured here experimentally for the first time.

Optically active III-V semiconductors quantum dots (QDs) are considered for applications in quantum information technologies and have major advantages, such as versatile device fabrication techniques and strong interaction between charge spin and light. However, magnetic coupling with the randomly polarized nuclei of the QD, makes the spin state of the electron vulnerable to dephasing and decoherence [15]. It has been shown that preparation of the nuclear spins in a "narrowed" state [5, 16] with reduced fluctuations but without significant net polarization suppresses electron spin dephasing [17]. However the improvement is limited to what can be achieved with electron spin echo. A far more attractive approach is to induce nuclear spin bath polarization close to 100%, which would not only yield extreme "narrowing", but also open the way for a completely new regime where electron-nuclear spin system has bosonic properties and exhibits effects similar to cavity quantum electrodynamics – such a regime is itself a prerequisite for ambitious proposals to use nuclei for quantum memories [18] and simulators [7]. However, it proved difficult to achieve or even identify the obstacles to such 100% polarization. In QDs the complexity of the problem arises from the mesoscopic nature of the nuclear spin bath: the typical number of spins $10^4 - 10^6$ is too large to access each individual nucleus, yet too small to ignore quantum correlations, coherence and fluctuations [11–13]. The problem is complicated further by inhomogeneity of the electron-nuclear interaction within the QD volume.

In QDs the degree of nuclear spin polarization P_N was previously estimated [8] by measuring the resulting hyperfine shift E_hf, which is the change in the energy splitting of the $S_\mathrm{z} = \pm 1/2$ electron spin levels. The shift produced by each nuclear isotope is:

$$E_\mathrm{hf} = kAIP_\mathrm{N}, \tag{1}$$

where I is the nuclear spin, A is the hyperfine constant characterizing the isotope and material only, and k is a factor ($0 \leq k \leq 1$) describing the spatial non-uniformities of the nuclear polarization, electron envelope wavefunction, and chemical composition in a specific QD structure. While E_hf can be measured very accurately, the uncertainty in A and k, leads to uncertainty in P_N. Here we demonstrate measurement of P_N not relying on assumptions about A and k, but based on direct mapping of the spin-3/2 eigenstate populations. Notably, this allows Eq. 1 to be factorised leading to an accurate value for A which have not yet been measured experimentally despite GaAs being one of the most important semiconductors.

We achieve $P_\mathrm{N} \approx 80\%$ and spin temperature $T_\mathrm{N} \approx 1.3$ mK at a bath temperature of $T = 4.2$ K. The observed P_N exceeds the predicted values for the quantum limit for nuclear spin cooling [12, 13] and further experiments rule out the coherent "dark" nuclear spin states as a single fundamental obstacle. Instead we expect the currently achieved P_N to be limited by competing contributions of nuclear spin pumping and depolarization mechanisms – with a further effort in designing the nuclear spin cooling protocol these obstacles can be overcome, potentially opening the way for achieving nuclear polarizations close to 100%.

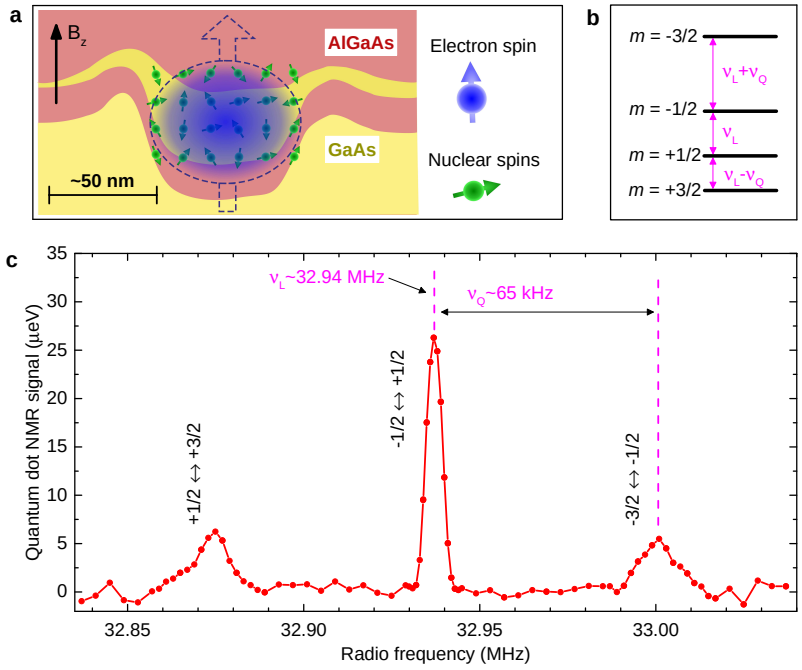

FIG. 1. **Electron and nuclear spins in quantum dots. a,** Schematic of a nanohole in-filled GaAs/AlGaAs quantum dot. An electron (blue) with spin S=1/2 trapped in the dot interacts with $> 10^4$ nuclear spins (green), each possessing a nuclear spin I=3/2 for gallium and arsenic, or I=5/2 for aluminium. **b,** Energy levels of a nuclear spin I=3/2 have distinct spin projections m along magnetic field B_z. Level splitting is dominated by the Zeeman effect (characterized by Larmor frequency $\nu_{\rm L} \propto B_z$), while qadrupolar effects cause additional changes in energies (characterized by frequency $\nu_{\rm Q}$ with $\nu_{\rm Q} \ll \nu_{\rm L}$). **(c,)** Nuclear magnetic resonance (NMR) spectrum measured on ^{75}As nuclei of a single QD B1 at $B_z \approx$4.5 T: transitions between individual levels m are clearly resolved due to quadrupolar effects induced by stressing the sample along the [110] direction. The Larmor and quadrupolar frequencies are found to be $\nu_{\rm L} \approx 32.94$ MHz and $\nu_{\rm Q} \approx 65$ kHz respectively.

We study individual GaAs/AlGaAs QDs grown by in-situ nanohole etching and filling [19]. A schematic cross-section of such a QD is shown in Fig. 1a. An individual electron with spin S=1/2 can be trapped in a QD typically consisting of $\sim 10^5$ atoms with predominantly I=3/2 nuclear spins. The hyperfine coupling (electron-nuclear magnetic interaction) has a dual effect of enabling polarization (cooling) of the nuclear spin by optically polarized electrons and providing a mechanism for optical probing of the net nuclear polarization via detection of the hyperfine shift $E_{\rm hf}$ (see Eq. 1) in the QD luminescence spectrum [8, 9]. (Further details on techniques can be found in Methods and Supplementary Notes 1 and 2.)

All experiments are performed at magnetic field $B_{\rm z} >$ 4 T along the sample growth axis (z) – the resulting Zeeman shifts $mh\nu_{\rm L}$ (h is Planck's constant) dominate the nuclear spin energy level structure (Fig. 1b), the spin states have well-defined projections m along the z-axis, and the frequencies of all dipole-allowed transitions $m \leftrightarrow m+1$ equal the Larmor frequency $\nu_{\rm L} = \gamma_{\rm N} B_{\rm z}/(2\pi)$ ($\gamma_{\rm N}$ is the nuclear gyromagnetic ratio). Strain induced quadrupolar effects give rise to small additional shifts $m^2 h\nu_{\rm Q}/2$ leading to a triplet of dipole-allowed transitions with splitting $\nu_{\rm Q}$. The transition frequencies are probed by measuring the nuclear magnetic resonance (NMR) spectrum as shown in Fig. 1c. Two features of the spectrum are important for this work: (i) $\nu_{\rm Q} \ll \nu_{\rm L}$ in a wide range of magnetic fields, so that the nuclear spin levels are nearly equidistant allowing straightforward use of the nuclear spin temperature concept [14, 20], (ii) the NMR triplet is well resolved, providing access to individual spin transitions and eventually allowing the spin temperature to be measured.

The collective state of the nuclear spin bath induced via optical cooling can be characterized by the population probabilities p_m of the levels with spin projections m. In thermal equilibrium the system is described by the canonical Boltzmann distribution:

$$p_m = e^{m\beta} / \sum_{m=-I}^{+I} e^{m\beta}, \qquad (2)$$

where dimensionless inverse temperature $\beta = h\nu_L/k_{\rm b}T_{\rm N}$ is introduced and $k_{\rm b}$ is the Boltzmann constant. For spin I=1/2 any statistical distribution is described by Eq. 2 with some $T_{\rm N}$. However, for $I >$1/2 the nuclear spin temperature hypothesis of Eq. 2 is a non-trivial statement implying existence of equilibration mechanisms which in turn require sufficiently "complex" interactions that can

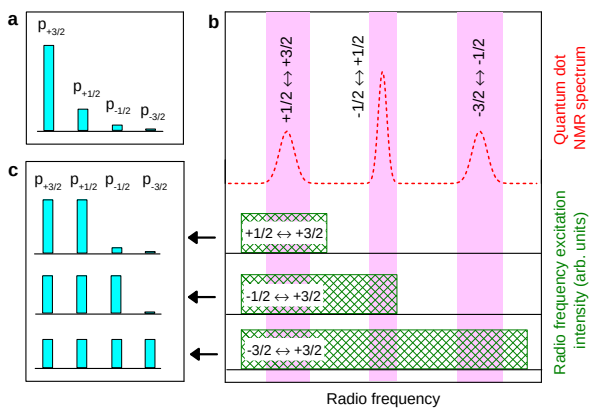

FIG. 2. **Manipulation of the nuclear spin states in quantum dots. a,** Population probabilities p_m of the nuclear spin levels with $m = -3/2..+3/2$ corresponding to Boltzmann distribution with polarization degree $P_N \approx +80\%$. **b,** Schematic NMR spectrum of the spin-3/2 nuclei (dashed line) and the rectangular spectral bands of the radio frequency (rf) magnetic field used for selective saturation of the NMR transitions. **c,** Modified population that result from the initial distribution **a** upon application of the corresponding rf band in **b**. For example, selective saturation of the $+1/2 \leftrightarrow +3/2$ NMR transition equalizes the $p_{+1/2}$ and $p_{+3/2}$ populations without affecting $p_{-1/2}$ and $p_{-3/2}$, while saturation of all three transitions equalizes all p_m. Such measurements produce optically detected hyperfine shifts proportional to various linear combinations of p_m, combined together, they allow for the statistical distribution p_m of the optically cooled nuclei to be reconstructed.

couple all states of the system leaving the total energy as the only constant of motion [14]. The polarization degree

$$P_N = \sum_{m=-I}^{+I} m p_m / I. \qquad (3)$$

is uniquely related to β and T_N when p_m are given by Eq. 2. An example of a Boltzmann distribution with $P_N \approx +80\%$ is sketched in Fig. 2a for I=3/2: most nuclei are in a $m = +3/2$ state with less than 2% occupying the $m = -3/2$ state.

We probe p_m distribution by manipulating it with radio-frequency (rf) pulses as demonstrated in Figs. 2b,c. This is possible since the optically-detected hyperfine shift depends on P_N and hence on p_m (Eqs. 1, 3). For example, a long rf pulse exciting selectively the $+1/2 \leftrightarrow +3/2$ NMR transition equalizes the $p_{+1/2}$ and $p_{+3/2}$ populations. The resulting change in hyperfine shift $\Delta E_{hf}^{+1/2 \leftrightarrow +3/2} = -kA(p_{+3/2} - p_{+1/2})/2$ is proportional to the difference $p_{+3/2} - p_{+1/2}$ of the *initial* state. In a similar way, the hyperfine shifts arising from saturation of one, two or three NMR transitions can be calculated (see Methods) and combined to reconstruct the statistical distribution p_m produced by optical cooling.

This approach is demonstrated experimentally in Figs. 3a,b for ^{75}As nuclei in QD B1. After optical cooling with light of a variable circular polarization degree, rf is applied to saturate selectively one or two NMR transitions. The resulting changes in hyperfine shifts $\Delta E_{hf}^{m \leftrightarrow m+1}$ and $\Delta E_{hf}^{m \leftrightarrow m+2}$ are shown by the symbols versus the total ^{75}As hyperfine shift $\Delta E_{hf}^{-3/2 \leftrightarrow +3/2}$ variation measured by saturating three NMR transitions. The pronounced non-linearities in the data are a clear signature of large, comparable to unity $|P_N|$, since at $|P_N| \ll 1$ (high temperature limit) all exponents $e^{m\beta}$ in Eq. 2 tend to $1 + m\beta$ and non-linearities vanish. For quantitative analysis we combine Eqs. 1, 3 and the spin temperature hypothesis of Eq. 2 (see derivation in Methods) and use kA product as the sole fitting parameter. For QD B1 all five model curves (shown by the lines in Figs. 3a,b) are in good agreement with experiment for $kA = 36.9 \pm 1.6$ μeV (95% confidence interval). This confirms the validity of the spin temperature hypothesis for the optically cooled nuclei. The smallest observed absolute temperature is found to be $T_N \approx \pm 1.3$ mK for ^{75}As at $B_z = 4.5$ T corresponding to $P_N \approx \pm 74\%$.

The measurements of Fig. 3b were repeated on different isotopes in several QDs each time in good agreement with the spin temperature hypothesis. The derived polarizations P_N of the individual isotopes are shown in Fig. 3c (top scale) as a function of the total hyperfine shift of all isotopes in dot B1. Similar results for another QD A1 at $B_z = 8.0$ T are shown as well (bottom scale) demonstrating P_N up to $\sim \pm 80\%$ (corresponding to $T_N \approx +2.0$ mK for ^{75}As). To our knowledge $P_N \approx 80\%$ is the largest reported for III-V QDs. Two factors are at play here: (i) The efficiency of nuclear spin cooling in the studied GaAs/AlGaAs nanohole dots is somewhat higher than in the previous studies: for example, the total hyperfine shifts $E_{hf} = \pm 100$ μeV observed here (Fig. 3c) can be directly compared to $E_{hf} = \pm 90$ μeV observed in GaAs/AlGaAs fluctuation dots [8]. (ii) What is more important, our measurement of P_N does not depend on the uncertainties in hyperfine constants A and dot structural parameter k – it is likely that P_N was underestimated in earlier studies.

From Fig. 3(c) we find that optical cooling produces the same P_N for all isotopes. Since the Larmor frequencies ν_L of the isotopes are significantly different (a factor of $\sim$1.78 for ^{71}Ga and ^{75}As) their spin temperatures T_N are different too. In other words, optical cooling leaves the Zeeman reservoir of each isotope in a state of internal thermal equilibrium, but out of equilibrium with other isotopes. Detailed measurements show that while T_N changes, under given optical pumping conditions the inverse temperature β is nearly invariant for different isotopes and magnetic fields $B_z = 4.5 - 8.5$ T (with maximum $|\beta| \approx 1.43$ corresponding to $P_N \approx 80\%$). This can be understood assuming that optical cooling of the nuclei arises purely from the hyperfine flip-flops: the change in

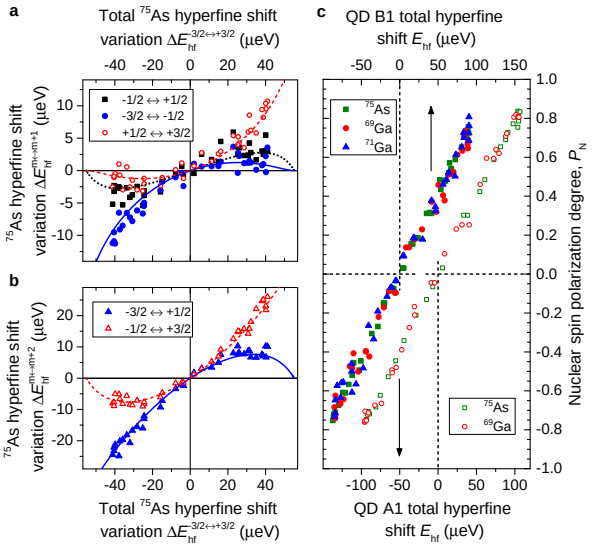

FIG. 3. **Probing nuclear spin temperature in a quantum dot. a,** Symbols show hyperfine shifts induced by selective saturation of each of the three dipolar NMR transitions of the spin-3/2 ^{75}As nuclei as a function of the hyperfine shift measured by simultaneous saturation of all NMR transitions in an individual QD B1 at B_z ≈4.5 T. **b,** Same experiment with simultaneous saturation of two NMR transitions provides better signal to noise ratio. Lines in **a** and **b** show model calculation with hyperfine constant as the only fitting parameter. The largest polarization of ^{75}As achieved in this experiment $P_N \approx \pm 74\%$ corresponds to nuclear spin temperature $T_N \approx \pm 1.3$ mK. **c,** polarization degree P_N of each isotope as a function of the total hyperfine shift E_{hf} of all isotopes in QD B1 (top scale, full symbols, B_z =4.5 T) and A1 (bottom scale, open symbols, B_z =8.0 T). All experimental plots in (**a-c**) are obtained by varying the degree of circular polarization of the optical pumping.

the electron spin projection S_z by ±1 is accompanied by a ∓1 change in the nuclear spin projection m, with each nucleus behaving independently, interacting only with the polarized electron spin [12, 21]. This leads to an invariant nuclear $p_{m+1}/p_m = e^{\beta}$ determined only by the electron spin properties. From the thermodynamics perspective, the isotopic difference in T_N can be seen to result from the insufficient "complexity" of the electron-nuclear flip-flop process: in particular it does not provide enough interaction pathways to equilibrate the Zeeman reservoirs of different isotopes.

The above findings are contrary to the theoretical predictions that quantum coherence between different nuclei gives rise to so-called nuclear "dark" states, limiting the maximum achievable $|P_N|$ in QDs [11–13]. It has been proposed that dark states can be disrupted by small perturbations of the electron wavefunction [11, 12] or simply by the nuclear-nuclear dipolar interaction [12]. Here we perform experiments where optical pumping is blocked periodically (which empties the dot) with off-times up to 120 ms. Such off-times exceed notably the nuclear spin transverse relaxation time $T_2 < 5$ ms (Ref. [22]) ensuring complete decoherence of the nuclei and disruption of the dark states via dipole-dipole interaction. On the other hand, off-times are much shorter than the nuclear spin longitudinal relaxation time $T_1 > 500$ s (Ref. [23]) minimizing any decay of $|P_N|$. However, pumping interruption was found to have no effect on P_N suggesting that nuclear dark states are not a limiting factor for achieving $|P_N|$ up to 80%. Evidently, there are intrinsic mechanisms disrupting nuclear spin coherence – inhomogeneity of the hyperfine interaction is the well understood one [12], while other, yet unexplored factors may include inhomogeneous quadrupolar shifts, or fluctuating electric fields arising from optically generated charges in neighboring QDs or traps.

With "dark" nuclear states ruled out for the studied structures, it is important to understand what limits $|P_N|$ at ≈80% and hence find a way to achieve $|P_N|$ ≈100%. Here we limit ourselves to varying the parameters in the particular cooling scheme used in this work, which employs optical pumping with a continious-wave multimode laser (linewidth ∼4 GHz). We find that the largest $|P_N| \approx 80$ % (as in Fig. 3) is achieved by exciting ∼55 meV above the exciton ground state (see Supplementary Note 3). Under such conditions, the limitations to $|P_N|$ may arise from the loss of electron spin polarization during energy relaxation, and competing effects of heavy and light hole excitation [24]. Moreover the maximum $|P_N|$ is observed under optical excitation powers ∼1000 times larger than the saturation power of the QD photoluminescence, i.e. spin cooling may be related to multiexciton complexes rather than the ground state exciton. Under such conditions optically induced nuclear spin relaxation [25] could be a significant limiting factor, whereas tunneling of the electrons through the thin (7nm) AlGaAs bottom barrier may increase $|P_N|$ by enabling fast recycling of the spin-polarized electrons through the QD. Additional studies are needed to explain why the nuclear spin cooling scheme used here is most efficient at such high optical powers and excess photon energies. However, the nuclear spin temperature measurement techniques presented here are not limited to the particular cooling mechanism and can be readily used to explore alternative cooling protocols.

We finally discuss the measurement of GaAs hyperfine constants A. In free atoms, where electron wavefunctions have an analytical form, A can be predicted accurately, while in the solid state, the effects of bonding and hybridization make quantitative predictions challenging [26]. The manifestations of the hyperfine interaction depend on the solid state system: for individual electron and nuclear spins in defects, a complex energy spectrum is observed [27], whereas electrons in III-V semiconductor nanostructures interact with a large number of nuclei leading to a simplified mean-field picture (Eq. 1) de-

termined by a single hyperfine parameter A defined as [28, 29]

$$A = (2\mu_0/3)\hbar\gamma_{\rm N} g_{\rm e}\mu_{\rm b}|\psi(0)|^2, \quad (4)$$

where $g_{\rm e} \approx 2$ is the free electron g-factor, μ_0 is magnetic constant, $\mu_{\rm b}$ is Bohr magneton, $\hbar = h/(2\pi)$, and the electron wavefunction density $|\psi(0)|^2$ at the nucleus is the only parameter characterizing the material (GaAs). By definition, fully polarized ($|P_{\rm N}| = 1$) spin-I nuclei produce electron hyperfine shift $E_{\rm hf} = AI$ regardless of the electron envelope wavefunction [29]. However, the effective hyperfine constant kA obtained from experiment on QDs is reduced by a factor $k \leq 1$ which includes the non-uniformity of the wavefunction and nuclear polarization.

Analysis presented in Supplementary Note 4 and based on the measurements of kA in dots with different electron confinement, shows that the spatial non-uniformity of $P_{\rm N}$ requires a correction of $\sim$ 10%, which when applied leads to the 95%-confidence estimates $|\psi_{\rm As}(0)|^2$=(9.25±0.20)×10^{31} m^{-3} and $|\psi_{\rm Ga}(0)|^2$=(6.57±0.25)×10^{31} m^{-3}, corresponding to A=43.5±0.9 μeV (^{75}As), A=43.1±1.6 μeV (^{69}Ga), and A=54.8±2.1 μeV (^{71}Ga). These experimental values generally agree with the original estimates of Paget et al. [29] based on the studies on InSb [28]. On the other hand the ratio $|\psi_{\rm As}(0)|^2/|\psi_{\rm Ga}(0)|^2 \approx 1.41$ which has the highest experimental accuracy deviates from ∼1.69 of Ref. [29]: the directly measured A values can be used for a more accurate modeling of GaAs electronic band structure.

Previous extensive experiments on optical probing of the QD nuclear spins have been limited to the nuclear mean-field approach [15]. The nuclear spin thermometry reported here is the first study beyond this framework and provides new routes to understanding the microscopic state of the nuclear spin bath. Such understanding is key to developing a self-consistent fully quantum description of the QD electron-nuclear spin system, which is still lacking. The existing quantum models [5, 12, 13, 16] employ significant simplifications (e.g. small numbers of nuclei, often limited to I=1/2 spins) and are sensitive to input parameters (e.g. inhomogeneity of the hyperfine coupling) that are known only approximately. Our observations can be fed back to the existing models (e.g. to identify realistic parameters that would restrict nuclear "dark" states to polarizations exceeding 80%) and used to develop improved models. We also envisage further experimental developments. The spin thermometry techniques can be transferred to self-assembled dots where despite large inhomogeneous quadrupolar effects the $m = \pm 1/2$ subensemble can be used [22] to explore mesoscopic nuclear spin thermodynamics both in high magnetic fields as studied here, and in low fields where the spin temperature concept does not apply to the full spin 3/2 or 9/2 manifolds [30]. Further insights into the microscopic structure of the nuclear spin state can be achieved by exploring the correlations in the dipole-dipole interaction reservoir – its temperature can be probed via thermal mixing with the Zeeman energy reservoir [14], whose temperature can be detected reliably as shown here. Such nuclear-nuclear correlations have not been studied in QDs experimentally but are predicted to have strong impact on the coherent evolution of the electron-nuclear system [5].

[1] Atature, M., Dreiser, J., Badolato, A., Hogele, A., Karrai, K., and Imamoglu, A. Quantum-Dot Spin-State Preparation with Near-Unity Fidelity. *Science* **312**, 551–553 (2006).

[2] Jacques, V., Neumann, P., Beck, J., Markham, M., Twitchen, D., Meijer, J., Kaiser, F., Balasubramanian, G., Jelezko, F., and Wrachtrup, J. Dynamic polarization of single nuclear spins by optical pumping of nitrogen-vacancy color centers in diamond at room temperature. *Phys. Rev. Lett.* **102**, 057403 (2009).

[3] Falk, A. L., Klimov, P. V., Ivády, V., Szász, K., Christle, D. J., Koehl, W. F., Gali, A., and Awschalom, D. D. Optical polarization of nuclear spins in silicon carbide. *Phys. Rev. Lett.* **114**, 247603 (2015).

[4] Burkard, G., Loss, D., and DiVincenzo, D. P. Coupled quantum dots as quantum gates. *Phys. Rev. B* **59**, 2070–2078 (1999).

[5] Schliemann, J., Khaetskii, A. V., and Loss, D. Spin decay and quantum parallelism. *Phys. Rev. B* **66**, 245303 (2002).

[6] Kurucz, Z., Sørensen, M. W., Taylor, J. M., Lukin, M. D., and Fleischhauer, M. Qubit protection in nuclear-spin quantum dot memories. *Phys. Rev. Lett.* **103**, 010502 (2009).

[7] Roumpos, G., Master, C. P., and Yamamoto, Y. Quantum simulation of spin ordering with nuclear spins in a solid-state lattice. *Phys. Rev. B* **75**, 094415 (2007).

[8] Gammon, D., Efros, A. L., Kennedy, T. A., Rosen, M., Katzer, D. S., Park, D., Brown, S. W., Korenev, V. L., and Merkulov, I. A. Electron and nuclear spin interactions in the optical spectra of single GaAs quantum dots. *Phys. Rev. Lett.* **86**, 5176–5179 (2001).

[9] Chekhovich, E. A., Makhonin, M. N., Kavokin, K. V., Krysa, A. B., Skolnick, M. S., and Tartakovskii, A. I. Pumping of nuclear spins by optical excitation of spin-forbidden transitions in a quantum dot. *Phys. Rev. Lett.* **104**, 066804 (2010).

[10] Petersen, G., Hoffmann, E. A., Schuh, D., Wegscheider, W., Giedke, G., and Ludwig, S. Large nuclear spin polarization in gate-defined quantum dots using a single-domain nanomagnet. *Phys. Rev. Lett.* **110**, 177602 (2013).

[11] Imamoğlu, A., Knill, E., Tian, L., and Zoller, P. Optical pumping of quantum-dot nuclear spins. *Phys. Rev. Lett.* **91**, 017402 (2003).

[12] Christ, H., Cirac, J. I., and Giedke, G. Quantum description of nuclear spin cooling in a quantum dot. *Phys. Rev. B* **75**, 155324 (2007).

[13] Hildmann, J., Kavousanaki, E., Burkard, G., and Ribeiro, H. Quantum limit for nuclear spin polarization in semiconductor quantum dots. *Phys. Rev. B* **89**,

205302 (2014).
[14] Goldman, M. *Spin temperature and nuclear magnetic resonance in solids.* Oxford University Press, Oxford, (1970).
[15] Urbaszek, B., Marie, X., Amand, T., Krebs, O., Voisin, P., Maletinsky, P., Hoegele, A., and Imamoglu, A. Nuclear spin physics in quantum dots: An optical investigation. *Rev. Mod. Phys.* **85**, 79–133 (2013).
[16] Barnes, E., Cywiński, L., and Das Sarma, S. Nonperturbative master equation solution of central spin dephasing dynamics. *Phys. Rev. Lett.* **109**, 140403 (2012).
[17] Xu, X., Yao, W., Sun, B., Steel, D. G., Bracker, A. S., Gammon, D., and Sham, L. J. Optically controlled locking of the nuclear field via coherent dark-state spectroscopy. *Nature* **459**, 1105–1109 (2009).
[18] Schwager, H., Cirac, J. I., and Giedke, G. Quantum interface between light and nuclear spins in quantum dots. *Phys. Rev. B* **81**, 045309 (2010).
[19] Atkinson, P., Zallo, E., and Schmidt, O. G. Independent wavelength and density control of uniform GaAs/AlGaAs quantum dots grown by infilling self-assembled nanoholes. *J. Appl. Phys.* **112**, 054303 (2012).
[20] Paravastu, A. K. and Reimer, J. A. Nuclear spin temperature and magnetization transport in laser-enhanced NMR of bulk GaAs. *Phys. Rev. B* **71**, 045215 (2005).
[21] D'Yakonov, M. I. and Perel, V. I. Optical orientation in a system of electrons and lattice nuclei in semiconductors. theory. *Sov. Phys. JETP* **38**, 177 (1974).
[22] Chekhovich, E. A., Hopkinson, M., Skolnick, M. S., and Tartakovskii, A. I. Suppression of nuclear spin bath fluctuations in self-assembled quantum dots induced by inhomogeneous strain. *Nat Commun* **6**, 6348 (2015).
[23] Ulhaq, A., Duan, Q., Zallo, E., Ding, F., Schmidt, O. G., Tartakovskii, A. I., Skolnick, M. S., and Chekhovich, E. A. Vanishing electron g factor and long-lived nuclear spin polarization in weakly strained nanohole-filled GaAs/AlGaAs quantum dots. *Phys. Rev. B* **93**, 165306 (2016).
[24] Sesti, E. L., Wheeler, D. D., Hayes, S. E., Saha, D., Sanders, G. D., and Stanton, C. J. Assignments of transitions in optically-pumped NMR of GaAs/AlGaAs quantum wells on a bulk GaAs substrate. *Phys. Rev. B* **90**, 125301 (2014).
[25] Paget, D., Amand, T., and Korb, J.-P. Light-induced nuclear quadrupolar relaxation in semiconductors. *Phys. Rev. B* **77**, 245201 (2008).
[26] Van de Walle, C. G. and Blöchl, P. E. First-principles calculations of hyperfine parameters. *Phys. Rev. B* **47**, 4244–4255 (1993).
[27] Yin, C., Rancic, M., de Boo, G. G., Stavrias, N., McCallum, J. C., Sellars, M. J., and Rogge, S. Optical addressing of an individual erbium ion in silicon. *Nature* **497**, 91–94 (2013).
[28] Gueron, M. Density of the conduction electrons at the nuclei in indium antimonide. *Phys. Rev.* **135**, A200–A205 (1964).
[29] Paget, D., Lampel, G., Sapoval, B., and Safarov, V. I. Low field electron-nuclear spin coupling in gallium arsenide under optical pumping conditions. *Phys. Rev. B* **15**, 5780–5796 (1977).
[30] Maletinsky, P., Kroner, M., and Imamoglu, A. Breakdown of the nuclear-spin-temperature approach in quantum-dot demagnetization experiments. *Nat Phys* **5**, 407 – 411 (2009).

ACKNOWLEDGMENTS. The authors are grateful to Armando Rastelli (Linz), Yongheng Huo (Hefei) and Andreas Waeber (TU Munich) for fruitful discussions. This work has been supported by the EPSRC Programme Grant EP/J007544/1. E.A.C. was supported by a University of Sheffield Vice-Chancellor's Fellowship and a Royal Society University Research Fellowship.

AUTHOR CONTRIBUTIONS. E.Z., F.D. and O.G.S. designed and grew the samples. E.A.C. and A.U. developed the techniques and conducted the experiments. E.A.C. conceived the project and analyzed the data. E.A.C. and M.S.S. wrote the manuscript with input from all authors.

ADDITIONAL INFORMATION. Correspondence and requests for materials should be addressed to E.A.C. (e.chekhovich@sheffield.ac.uk).

DATA AVAILABILITY. The data that support the findings of this study are available from the corresponding author upon reasonable request.

METHODS

Experimental techniques. We use neutral quantum dots, i.e. without optical excitation the dots are empty. All experiments were conducted in a helium bath cryostat at T=4.2 K. In all measurements we use the *Optical cooling - rf depolarization - Optical readout* protocol described previously in detail [22, 31]. The rf depolarization is performed in the absence of optical excitation. The role of the short optical readout pulse is to excite photoluminescence whose spectrum is then analyzed with a double spectrometer and a CCD camera.

Photoluminescence of a neutral QD results from recombination of an electron with spin up ($\uparrow$) or down ($\downarrow$) and a hole with spin up ($\Uparrow$) or down ($\Downarrow$) along the sample growth direction (z axis). We observe emission of both the "bright" excitons $|\Uparrow\downarrow\rangle$, $|\Downarrow\uparrow\rangle$ and "dark" excitons $|\Uparrow\uparrow\rangle$, $|\Downarrow\downarrow\rangle$ that gain oscillator strength from the bright states due to the reduced quantum dot symmetry.

The net nuclear spin polarization shifts the energies of the exciton states. The shifts are dominated by the sign of the electron spin z projection, they are $\approx +E_{\rm hf}/2$ for $|\Downarrow\uparrow\rangle$ and $|\Uparrow\uparrow\rangle$ states, and $\approx -E_{\rm hf}/2$ for $|\Uparrow\downarrow\rangle$ and $|\Downarrow\downarrow\rangle$ states. In order to determine $E_{\rm hf}$ accurately we measure the energy difference of the $|\Downarrow\uparrow\rangle$ and $|\Downarrow\downarrow\rangle$ bright and dark states (or of the $|\Uparrow\uparrow\rangle$ and $|\Uparrow\downarrow\rangle$ dark and bright states). In this way we eliminate any contribution of the hole hyperfine interaction, as well as any simultaneous shifts of all exciton states arising e.g. from charge fluctuations in the dot vicinity.

The spectrum of Fig. 1c is obtained using "inverse" NMR method [31] and is averaged over two measurements with positive and negative nuclear polarization – in this way both $-3/2 \leftrightarrow -1/2$ and $+1/2 \leftrightarrow +3/2$ NMR transitions yield sufficient signal to be observed.

Relation between the nuclear spin population probabilities p_m and the optically detected hyperfine shifts. In experiments we use long and weak (no Rabi oscillations) radio frequency (rf) excitation. If rf is resonant with the NMR transition between states m and $m+1$ its effect is to change and equalize the populations of these states so that $p_m, p_{m+1} \to (p_m + p_{m+1})/2$, while population probabilities of all other nuclear spin states remain unchanged. One can then use Eqs 1 and 3 to calculate the change in the optically detected hyperfine shift $\Delta E_{\rm hf}$ arising from such manipulation of p_m. For example for $m = +1/2$ and $m+1 = +3/2$ we calculate as follows: $\Delta E_{\rm hf}^{+1/2 \leftrightarrow +3/2} = kA\left[(+\frac{3}{2})\frac{p_{+3/2}+p_{+1/2}}{2} + (+\frac{1}{2})\frac{p_{+3/2}+p_{+1/2}}{2}\right] - kA\left[(+\frac{3}{2})p_{+3/2} + (+\frac{1}{2})p_{+1/2}\right] = -kA(p_{+3/2} - p_{+1/2})/2$, i.e. the hyperfine shift $\Delta E_{\rm hf}$ depends only on the difference in the initial populations of the states excited with rf.

In a similar way, simultaneous saturation of the NMR transitions $m \leftrightarrow m+1$ and $m+1 \leftrightarrow m+2$ leads to the following redistribution of the populations: $p_m, p_{m+1}, p_{m+2} \to (p_m + p_{m+1} + p_{m+2})/3$. Saturation of all 3 NMR transition of spin I=3/2 nuclei leads to $p_{-3/2}, p_{-1/2}, p_{+1/2}, p_{+3/2} \to (p_{-3/2} + p_{-1/2} + p_{+1/2} + p_{+3/2})/4 = 1/4$, where the last equality is due to normalization $\sum_{m=-I}^{I} p_m = 1$. Using Eqs. 1, 3 we evaluate the changes in the hyperfine shift $\Delta E_{\rm hf}$ for each case:

$$\begin{aligned}
\Delta E_{\rm hf}^{m\leftrightarrow m+1} &= -kA(p_{m+1} - p_m)/2 = \\
&= -kA\frac{e^{(m+1)\beta} - e^{m\beta}}{4\cosh(\beta/2) + 4\cosh(3\beta/2)}, \\
\Delta E_{\rm hf}^{m\leftrightarrow m+2} &= -kA(p_{m+2} - p_m) = \\
&= -kAe^{(m+1)\beta}\sinh(\beta/2)/\cosh(\beta), \\
\Delta E_{\rm hf}^{-I\leftrightarrow +I} &= -kAP_{\rm N}I = \\
&= -kA[3/2 + 1/\cosh(\beta)]\tanh(\beta/2).
\end{aligned} \tag{5}$$

The last expression in each of these equations is obtained by substituting the Boltzmann distribution (Eq. 2).

Unlike $\Delta E_{\rm hf}^{m\leftrightarrow m+1}$ and $\Delta E_{\rm hf}^{m\leftrightarrow m+2}$, the $\Delta E_{\rm hf}^{-I\leftrightarrow +I}$ variation is a monotonic function of β with $\beta \in (-\infty, +\infty)$. It is thus possible to express β in terms of $\Delta E_{\rm hf}^{-I\leftrightarrow +I}$ and then substitute it into expressions for $\Delta E_{\rm hf}^{m\leftrightarrow m+1}$ and $\Delta E_{\rm hf}^{m\leftrightarrow m+2}$, eliminating β. Since there is no analytical solution we do this by making parametric plots of $\Delta E_{\rm hf}^{m\leftrightarrow m+1}$ and $\Delta E_{\rm hf}^{m\leftrightarrow m+2}$ as a function of $\Delta E_{\rm hf}^{-I\leftrightarrow +I}$ such as shown in Figs. 3a,b by the lines. The kA product is an overall scaling factor used as a parameter to fit the experimental data. One can see that such fitting can be achieved reliably only because large $P_{\rm N}$ is reached in experiment: only then there are pronounced asymmetries and nonlinearities in the $\Delta E_{\rm hf}^{m\leftrightarrow m+1}(\Delta E_{\rm hf}^{-I\leftrightarrow +I})$ and $\Delta E_{\rm hf}^{m\leftrightarrow m+2}(\Delta E_{\rm hf}^{-I\leftrightarrow +I})$ dependencies (observed in Figs. 3a,b). By contrast, in the high temperature limit ($\beta \to 0$, $P_{\rm N} \to 0$) Eq. 5 yields linear dependencies $\Delta E_{\rm hf}^{m\leftrightarrow m+1} = (1/10)\Delta E_{\rm hf}^{-I\leftrightarrow +I}$, $\Delta E_{\rm hf}^{m\leftrightarrow m+2} = (4/10)\Delta E_{\rm hf}^{-I\leftrightarrow +I}$ independent of m, so that experiment can be described with any kA, making fitting impossible.

Once kA is obtained from fitting, one can use the last of Eq. 5 to uniquely relate the experimentally measured $\Delta E_{\rm hf}^{-I\leftrightarrow +I}$, and the quantities of interest such as polarization degree $P_{\rm N}$, the inverse temperature β, and the nuclear spin temperature $T_{\rm N}$ itself.

[31] Chekhovich, E. A., Kavokin, K. V., Puebla, J., Krysa, A. B., Hopkinson, M., Andreev, A. D., Sanchez, A. M., Beanland, R., Skolnick, M. S., and Tartakovskii, A. I. Structural analysis of strained quantum dots using nuclear magnetic resonance. *Nature Nanotech.* **7**, 646–650 (2012).